Schouws, Sander, Bouwens, Rychard J., Ormerod, Katherine, Smit, Renske, Algera, Hiddo, Sommovigo, Laura, Hodge, Jacqueline, Ferrara, Andrea, Oesch, Pascal A., Rowland, Lucie E., van Leeuwen, Ivana, Stefanon, Mauro, Herard-Demanche, Thomas, Fudamoto, Yoshinobu, Röttgering, Huub and van der Werf, Paul

Detection of [O iii] 88 μ m in JADES-GS-z14-0 at z = 14.1793

The Astrophysical Journal, 988:19 (8pp), 2025 July 20 https://doi.org/10.3847/1538-4357/adbf1b

Detection of $[O\,III]_{88\,\mu m}$ in JADES-GS-z14-0 at $z = 14.1793$

Sander Schouws[1], Rychard J. Bouwens[1], Katherine Ormerod[2], Renske Smit[2], Hiddo Algera[3,4], Laura Sommovigo[5], Jacqueline Hodge[1], Andrea Ferrara[6], Pascal A. Oesch[7,8,9], Lucie E. Rowland[1], Ivana van Leeuwen[1], Mauro Stefanon[1], Thomas Herard-Demanche[1], Yoshinobu Fudamoto[10], Huub Röttgering[1], and Paul van der Werf[1]
[1] Leiden Observatory, Leiden University, NL-2300 RA Leiden, The Netherlands
[2] Astrophysics Research Institute, Liverpool John Moores University, 146 Brownlow Hill, Liverpool L3 5RF, UK
[3] Hiroshima Astrophysical Science Center, Hiroshima University, 1-3-1 Kagamiyama, Higashi-Hiroshima, Hiroshima 739-8526, Japan
[4] National Astronomical Observatory of Japan, 2-21-1, Osawa, Mitaka, Tokyo, Japan
[5] Center for Computational Astrophysics, Flatiron Institute, 162 Fifth Avenue, New York, NY 10010, USA
[6] Scuola Normale Superiore, Piazza dei Cavalieri 7, 50126 Pisa, Italy
[7] Departement d'Astronomie, Université de Genéeve, 51 Ch. des Maillettes, CH-1290 Versoix, Switzerland
[8] Cosmic Dawn Center (DAWN), Copenhagen, Denmark
[9] Niels Bohr Institute, University of Copenhagen, Jagtvej 128, DK-2200 Copenhagen N, Denmark
[10] Center for Frontier Science, Chiba University, 1-33 Yayoi-cho, Inage-ku, Chiba 263-8522, Japan
Received 2024 September 30; revised 2025 February 26; accepted 2025 March 9; published 2025 July 10

Abstract

We report the first successful Atacama Large Millimeter/submillimeter Array (ALMA) follow-up observations of a secure $z > 10$ JWST-selected galaxy, by robustly detecting (6.6σ) the $[O\,III]_{88\,\mu m}$ line in JADES-GS-z14-0 (hereafter GS-z14). The ALMA detection yields a spectroscopic redshift of $z = 14.1793 \pm 0.0007$, and increases the precision on the prior redshift measurement of $z = 14.32^{+0.08}_{-0.20}$ from NIRSpec by $\gtrsim$180×. Moreover, the redshift is consistent with that previously determined from a tentative detection (3.6σ) of $C\,III]_{1907,1909}$ ($z = 14.178 \pm 0.013$), solidifying the redshift determination via multiple line detections. We measure a line luminosity of $L_{[O\,III]88} = (2.1 \pm 0.5) \times 10^8\,L_\odot$, placing GS-z14 at the lower end, but within the scatter of, the local $L_{[O\,III]88}$–star formation rate relation. No dust continuum from GS-z14 is detected, suggesting an upper limit on the dust-to-stellar mass ratio of $<2 \times 10^{-3}$, consistent with dust production from supernovae with a yield $y_d < 0.3\,M_\odot$. Combining a previous JWST/MIRI photometric measurement of the [O III]$\lambda\lambda$4959,5007 Å and Hβ lines with CLOUDY models, we find GS-z14 to be surprisingly metal-enriched ($Z \sim 0.05$–$0.2\,Z_\odot$) a mere 300 Myr after the Big Bang. The detection of a bright oxygen line in GS-z14 thus reinforces the notion that galaxies in the early Universe undergo rapid evolution.

Unified Astronomy Thesaurus concepts: Galaxy evolution (594); High-redshift galaxies (734); Interstellar medium (847); Early universe (435)

1. Introduction

The discovery and spectroscopic confirmation of galaxies at $z > 10$ has recently become possible due to the groundbreaking capabilities offered by the James Webb Space Telescope (JWST; e.g., A. J. Bunker et al. 2023; E. Curtis-Lake et al. 2023; B. E. Robertson et al. 2023; S. Carniani et al. 2024; S. L. Finkelstein et al. 2024; J. A. Zavala et al. 2024). In particular, JADES-GS-z14-0 (hereafter GS-z14) was recently spectroscopically confirmed to be the most distant known galaxy at $z_{spec} = 14.32^{+0.08}_{-0.20}$, less than 300 Myr after the Big Bang (S. Carniani et al. 2024). Notably, GS-z14 is also very luminous with $M_{UV} = -20.81 \pm 0.16$, which makes it the second most luminous $z > 8$ galaxy with a spectroscopic redshift; only GN-z11 (P. A. Oesch et al. 2016; A. J. Bunker et al. 2023) is more luminous by a factor ∼2×.

Moreover, in contrast to other $z > 10$ galaxies, the rest-frame UV morphology of GS-z14 is extended and not highly concentrated. This implies that the luminosity is dominated by a spatially extended stellar population as opposed to an active galactic nucleus. The existence of objects like GS-z14 suggests a much more rapid build-up of galaxies in the very early Universe than previously expected (S. Carniani et al. 2024). GS-z14 enables a unique opportunity to study this rapid build-up in detail (A. Ferrara 2024).

The high luminosity of GS-z14 makes it an exceptional target for multiwavelength follow-up observations capable of revealing its physical conditions. Here we present new observations of GS-z14 targeting the luminous $[O\,III]_{88\,\mu m}$ far-infrared line with the Atacama Large Millimeter/submillimeter Array (ALMA).

The [O III] 88-micron fine-structure line is one of the dominant coolants of the interstellar medium (ISM). It originates from ionized gas in H II regions (D. Cormier et al. 2015), where ionizing radiation from young, massive stars has stripped electrons from oxygen atoms. Both semianalytical models (S. Yang & A. Lidz 2020; L. Vallini et al. 2021; L. Vallini et al. 2024) and radiative transfer postprocessed large box (K. Moriwaki et al. 2018), cosmological zoom-in (H. Katz et al. 2017; S. Arata et al. 2020; H. Katz et al. 2022; A. Pallottini et al. 2022; M. Kohandel et al. 2023; Y. Nakazato et al. 2023) hydrodynamical simulations have been employed to predict and interpret $[O\,III]_{88\,\mu m}$ emission in high redshift sources. The consensus is that bright $[O\,III]_{88\,\mu m}$ emission is generally associated with hard ionization fields (S. Yang & A. Lidz 2020; A. Pallottini et al. 2022), high ionization parameters (K. Moriwaki et al. 2018; S. Arata et al. 2020; Y. Nakazato et al. 2023; L. Vallini et al. 2024), and low metallicities (H. Katz et al. 2019; L. Vallini et al. 2024). These physical properties are likely to be ubiquitous in very actively

star-forming galaxies at high redshifts, making this line the ideal target for ALMA follow-up observations of JWST-selected $z > 10$ galaxies.

In the last two years, ALMA follow-up observations have been performed for several high-redshift galaxy candidates. GHZ2 (M. Castellano et al. 2022; C. T. Donnan et al. 2022; R. P. Naidu et al. 2022; R. Bouwens et al. 2023; Y. Harikane et al. 2023), with a photometric redshift of $z = 11.96$–12.42, was targeted with an ALMA Band 6 search for $[\mathrm{O\,III}]_{88\,\mu\mathrm{m}}$ by T. J. L. C. Bakx et al. (2023), who determined a 5σ upper limit of $\log(L_{[\mathrm{O\,III}]}/L_\odot) < 1.7 \times 10^8$ (see also G. Popping 2023). GHZ2 was later spectroscopically confirmed at $z = 12.34$ (M. Castellano et al. 2024), with J. A. Zavala et al. (2024) estimating a star formation rate (SFR) of $9 \pm 3\,M_\odot\,\mathrm{yr}^{-1}$ from the Hα line. Following its spectroscopic confirmation, J. A. Zavala et al. (2024) re-examined the ALMA observations of GHZ2 presented in T. J. L. C. Bakx et al. (2023), but were not able to identify a plausible $>5\sigma$ $[\mathrm{O\,III}]_{88\,\mu\mathrm{m}}$ detection at the expected frequency.

An ALMA line scan was also performed on GHZ1, with a photometric redshift of $z \approx 10.6$ (T. Treu et al. 2023), SFR of $36.3^{+54.5}_{-26.8}\,M_\odot\,\mathrm{yr}^{-1}$, and stellar mass $\log(M_\star/M_\odot) = 9.1^{+0.3}_{-0.4}$ (P. Santini et al. 2023), yielding a marginal $[\mathrm{O\,III}]_{88\,\mu\mathrm{m}}$ signal near its JWST position (I. Yoon et al. 2023) and an upper limit of $L_{[\mathrm{O\,III}]} < 2.2 \times 10^8 L_\odot$ (5σ). Another high-redshift candidate, HD1 at $z = 13.3$ (Y. Harikane et al. 2023) was observed in ALMA Bands 4 and 6 targeting $[\mathrm{C\,II}]_{158\,\mu\mathrm{m}}$ and $[\mathrm{O\,III}]_{88\,\mu\mathrm{m}}$, respectively, but the lines were not detected (M. Kaasinen et al. 2023). HD1 was later shown to be a low-redshift interloper at $z = 4.0$ (Y. Harikane et al. 2025). Finally, S5-z17-1, identified in JWST ERO data, showed a potential 5.1σ detection at 338.726 GHz, possibly corresponding to $[\mathrm{O\,III}]_{52\,\mu\mathrm{m}}$ at $z = 16$ (S. Fujimoto et al. 2023), suggesting an SFR $< 120\,M_\odot\,\mathrm{yr}^{-1}$. However, the high-redshift nature of this galaxy has not been conclusively established.

Overall, these upper limits and nondetections indicate possible lower redshift solutions or insufficient sensitivity in the requested observations (T. J. L. C. Bakx et al. 2023; S. R. Furlanetto & J. Mirocha 2023; M. Kaasinen et al. 2023). However, the burstiness of star formation (SF) in such high-redshift galaxies, as well as the impact of feedback processes on galaxy spectra and visibility, have also been suggested as physical motivations for the lack of ALMA detections at $z > 10$ (M. Kohandel et al. 2023; Y. Nakazato et al. 2023).

Throughout this paper, we assume a standard ΛCDM cosmology with $H_0 = 70\,\mathrm{km\,s^{-1}\,Mpc^{-1}}$, $\Omega_m = 0.3$, and $\Omega_\Lambda = 0.7$. Magnitudes are presented in the AB system (J. B. Oke & J. E. Gunn 1983). For star formation rates and stellar masses, we adopt a Chabrier initial mass function (IMF; G. Chabrier 2003). Error bars indicate the 68% confidence interval unless specified otherwise. All measured and derived physical quantities are corrected for gravitational lensing by a factor of $1.17\times$ (S. Carniani et al. 2024). Logarithms use base 10 unless specified otherwise.

2. Observations and Data Reduction

2.1. JWST

GS-z14 was discovered in deep imaging of the GOODS-South field obtained by the JWST Advanced Deep Extragalactic Survey (JADES; D. J. Eisenstein et al. 2023a) and the First Reionization Epoch Spectroscopic COmplete Survey (FRESCO; P. A. Oesch et al. 2023). GS-z14 was initially flagged as a likely low redshift interloper (K. N. Hainline et al. 2024; C. C. Williams et al. 2024) due to a nearby foreground galaxy at $z = 3.475$ with a separation of only $0\farcs4$, and due to its high luminosity. However, further analysis, including additional medium-band observations, favored a high redshift solution (B. E. Robertson et al. 2023).

Deep follow-up spectroscopy with NIRSpec presented in S. Carniani et al. (2024) shows a strong break at $\sim 1.85\,\mu$m, consistent with a Lyman break at $z \sim 14$. The profile of the Lyman break is sensitive to absorption of hydrogen along the line of sight, neutral gas in the galaxy and environment, velocity offsets, the presence of Lyα emission and possible ionized bubbles. Accounting for these effects, S. Carniani et al. (2024) determined a spectroscopic redshift of $z = 14.32^{+0.08}_{-0.20}$.

In contrast to other $z > 10$ sources, the spectrum of GS-z14 does not contain strong rest-frame UV emission lines. Only C III]$\lambda\lambda$1907,9 Å is tentatively detected with a significance of 3.6σ at $z = 14.178 \pm 0.013$, consistent with the redshift obtained from the Lyman Break. S. Carniani et al. (2024) discuss a number of mechanisms that could be responsible for the lack of strong emission lines in the rest-frame UV, ranging from a sudden quenching of the star formation, very low or high metallicities ($Z < 0.05\,Z_\odot$ or $Z \sim Z_\odot$), a high escape fraction of ionizing photons, and a difference in the dominant ionizing flux.

Interestingly, GS-z14 is also detected by MIRI in the F770W filter (J. M. Helton et al. 2024). This filter covers the rest-frame optical emission of GS-z14, corresponding to wavelengths of 4.4–5.7 μm. This part of the spectrum contains the strong [O III]$\lambda\lambda$4959,5007 Å and Hβ emission lines, and indeed the observed flux is significantly stronger than observed in the adjacent F444W filter, implying a significant contribution from the emission lines (constituting about one-third of the total F770W flux).

Spectral energy distribution (SED) fitting of GS-z14 performed by J. M. Helton et al. (2024) shows that the photometry is consistent with a stellar mass of $\log(M_*/M_\odot) = 8.7^{+0.5}_{-0.4}$. The models estimate that most of this stellar mass was formed relatively recently, with a mass-weighted age of $\sim$20 Myr. J. M. Helton et al. (2024) determine the current (<10 Myr) star formation rate of GS-z14 to be $25^{+6}_{-5}\,M_\odot\,\mathrm{yr}^{-1}$—consistent with the measurement of $22 \pm 6\,M_\odot\,\mathrm{yr}^{-1}$ from S. Carniani et al. (2024). Combined with the measured size of 260 ± 20 pc, this implies a high star formation rate surface density of $\sim 64\,M_\odot\,\mathrm{yr}^{-1}\,\mathrm{pc}^{-2}$, comparable to intense starbursting galaxies in the local Universe (R. Genzel et al. 2010). The UV slope $\beta_{\mathrm{UV}} = -2.20 \pm 0.07$ indicates the presence of a moderate amount of dust in addition to the very young stellar population, with a visual extinction of $A_V = 0.31^{+0.14}_{-0.07}$ (S. Carniani et al. 2024). Finally, the metallicity is poorly constrained owing to a lack of detected emission lines, but is expected to be low ($Z = 0.014^{+0.052}_{-0.012}\,Z_\odot$; S. Carniani et al. 2024).

2.2. ALMA

The ALMA Band 6 follow-up observations targeting the $[\mathrm{O\,III}]_{88\,\mu\mathrm{m}}$ line were obtained as part of a Cycle 10 Director's Discretionary Time (DDT) program (#2023.A.00037.S, PI: Schouws). An observing set-up using two tunings with three spectral windows each was utilized to maximize the coverage of the redshift likelihood distribution derived from the spectroscopic Lyman break. This results in a continuous

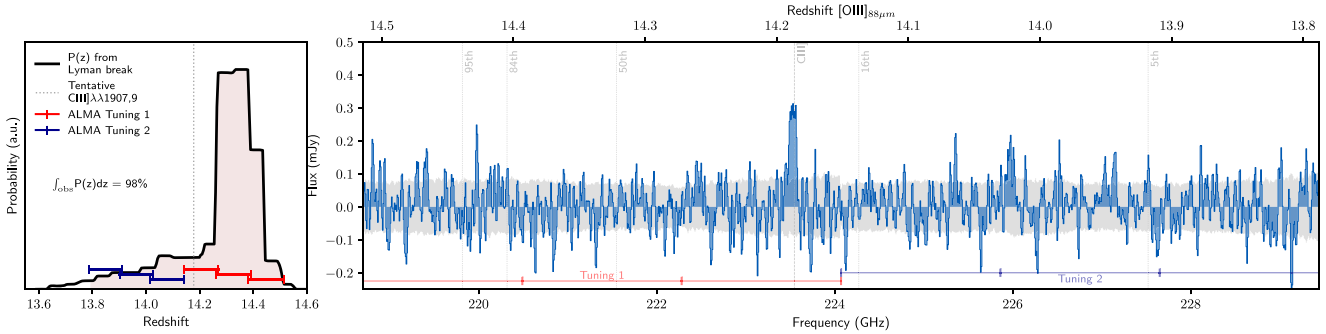

Figure 1. Left panel: the ALMA observations cover 98% of the redshift probability distribution derived from the Lyman break as observed by NIRSpec PRISM. We use two tunings with three spectral windows each, tuning 1 and 2 cover 83% and 15% of the probability distribution, respectively. Right panel: flux constraints extracted at the position of GS-z14 (blue histogram) vs. frequency from the 2023.A.00037.S spectral scan observations. The gray contours indicate the 1σ uncertainties. For context, we show the expected redshift from the tentative C III]$_{1907,1909}$ line from NIRSpec as well as the 5th, 16th, 50th, 86th, and 95th percentiles of the $P(z)$ distribution. There is only one feature in the line scan that can be confidently identified as [O III]$_{88\ \mu m}$ line emission, and it occurs at a frequency of 223.528 ± 0.009 GHz.

frequency coverage ranging from 218.70 to 229.45 GHz, corresponding to a redshift range of $z = 13.79$–14.51. We show in Figure 1 that the observing strategy covers 98% of the $P(z)$.

The observations for tuning 2 were carried out between 2024 August 15 and 16 in good weather conditions (precipitable water vapor, PWV = 0.67 mm), achieving the requested sensitivity in 2.8 hr. Tuning 1 was observed between 2024 September 7 and 8 for 2.8 hr in excellent conditions (PWV = 0.30 mm). Both tunings were observed with different array configurations due to scheduling constraints. Tuning 1 was observed in C-4 and tuning 2 in C-5 with baselines of 15–500 and 15–919 m, resulting in synthesized beams of 1.″09 × 0.″81 and 0.″57 × 0.″49, respectively, when using natural weighting.

The ALMA data were reduced and calibrated following the standard ALMA pipeline procedures with the Common Astronomy Software Applications (v6.5.4-9; CASA; T. R. Hunter et al. 2023). The amplitude and phase calibrations were performed using J0334-4008 and J0348-2749, respectively. Both calibrators are part of the ALMA Calibrator Source Catalog and are therefore considered reliable for Band 6 observations. Under typical conditions, the absolute flux calibration accuracy for Band 6 is 5%–10% (ALMA Technical Handbook 2024). The data were well behaved, with no bad antennas or channels requiring flagging.

The resulting calibrated measurement sets were time-averaged in bins of 30 s to reduce the data size, after carefully verifying that time-average smearing does not impact our results (e.g., A. R. Thompson et al. 2017).

Imaging of the calibrated visibilities was performed with natural weighting using the TCLEAN task in CASA, cleaning to a depth of 2σ using automasking (A. A. Kepley et al. 2020). We use a pixel scale of 0.″076 to properly sample the synthesized beam, which has a FWHM of 1.″08 × 0.″80 at the frequency of the [O III]$_{88\ \mu m}$ line.

2.3. Line Search

We perform a blind search for emission lines using an algorithm similar to the one used by M. Béthermin et al. (2020) for the ALPINE survey (A. L. Faisst et al. 2020; O. Le Fèvre et al. 2020) and S. Schouws et al. (2025, in preparation) for the REBELS survey (R. J. Bouwens et al. 2022). The algorithm loops over all channels and collapses moment maps over a range of 75–350 km s^{-1} in steps of one channel (∼10 km s^{-1}). For each moment map, we identify the significant ($>3\sigma$) peaks and add the results to a large list of features. This list is then pruned by removing duplicates within 2 × FWHM and 1.5× the beam size. We also perform the search on the negative moment map, which is useful to characterize the noise properties. In Figure 1, we show a blind extraction of the ALMA spectrum at the location of GS-z14 using a 0.″5 aperture.

The most significant line candidate we extract within a 0.″5 radius of the JWST position of GS-z14 is detected with a peak significance of 6.6σ and separation of 0.″12. The candidate line is consistent with being spatially coincident with GS-z14 in the JWST/NIRCam observations, given expected 0.″18 positional uncertainties following from a 6.6σ line detection and 1.″08 beam.[11]

3. Results

3.1. [O III]$_{88\ \mu m}$ in GS-z14

We have identified an emission line with a signal-to-noise of 6.6σ within 0.″12 of GS-z14 at 223.528 ± 0.009 GHz. This corresponds to [O III]$_{88\ \mu m}$ at $z = 14.1793 \pm 0.0007$, consistent with both the redshift derived from the Lyman break observed by JWST and also the tentative 3.6σ detection of C III]$_{1907,1909}$ at 2.89 μm (S. Carniani et al. 2024). In particular, the consistency of our new redshift determination from [O III]$_{88\ \mu m}$ with the earlier redshift estimate $z = 14.178 \pm 0.003$ from the tentative C III]$_{1907,1909}$ doublet (S. Carniani et al. 2024) greatly increases our confidence in the robustness of the current redshift determination given the availability of multiple line detections. We show the contours of the [O III]$_{88\ \mu m}$ emission overlaid on an RGB image based on F150W, F200W, and F400W imaging and a signal-to-noise-optimized extraction of the spectrum in Figure 2.

We measure the integrated line flux using the moment-zero map of the emission line, including all channels that fall within 2× the FWHM of the line. The FWHM is determined in an iterative process; starting from an estimate of the FWHM, we collapse a moment-zero map and extract a 1D spectrum, which is extracted by including all pixels with signal-to-noise ratio $>3\sigma$ on the moment-zero map. A new FWHM is then measured using this 1D spectrum by fitting a Gaussian. This

[11] https://help.almascience.org/kb/articles/what-is-the-absolute-astrometric-accuracy-of-alma

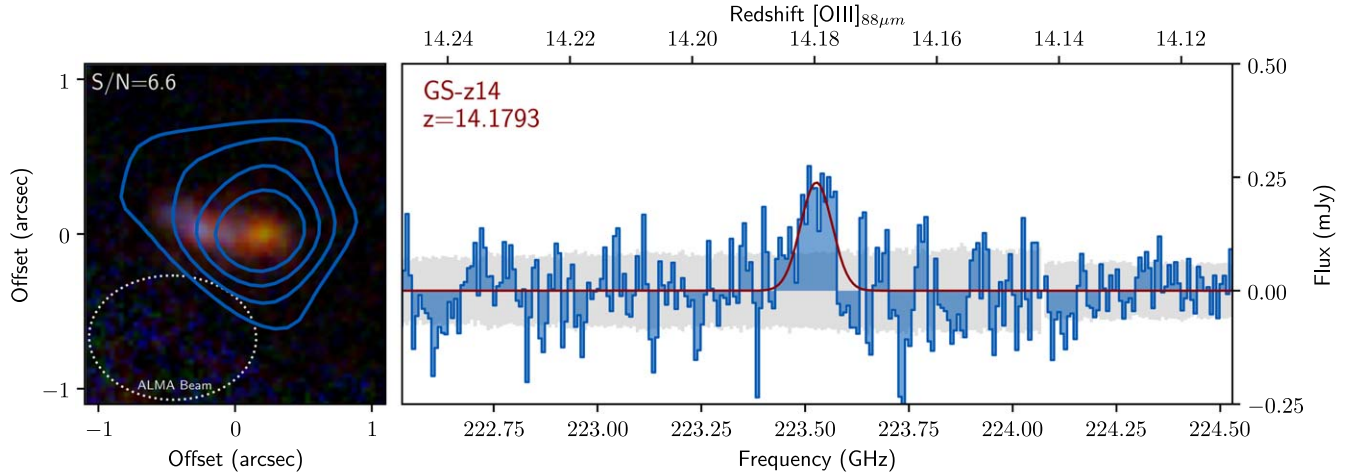

Figure 2. Detection of [O III]$_{88\ \mu m}$ in GS-z14 at $z = 14.1793 \pm 0.0007$. Left panel: contours showing the [O III]$_{88\ \mu m}$ emission (2σ, 3σ, 4σ, and 5σ) overlaid on an RGB image based on F150W, F200W, and F444W imaging (D. J. Eisenstein et al. 2023a, 2023b). The object with a bluer color to the left of GS-z14 is a $z = 3.475$ foreground galaxy (S. Carniani et al. 2020). The [O III]$_{88\ \mu m}$ emission is detected at a peak significance of 6.6σ in the collapsed data cube and well centered on GS-z14. Right panel: the spectrum of the [O III]$_{88\ \mu m}$ line (blue bars) extracted from the $>3\sigma$ emission region in the moment-zero map. The red line shows the Gaussian fit used to measure the spectroscopic redshift and FWHM of the line. The gray shaded region indicates the 1σ uncertainties.

new FWHM is then used to collapse a new moment-zero map for the next iteration. A stable FWHM is achieved in less than 10 steps (S. Schouws et al. 2022).

The final FWHM we measure is 136 ± 31 km s^{-1}. Assuming that GS-z14 is dispersion-dominated and $r_{[O\ III]} = r_e = 260$ pc, this implies a dynamical mass of $(1.0 \pm 0.5) \times 10^9\ M_\odot (\sin i)^2$. At the current resolution, we do not see evidence for a velocity gradient.

We measure an integrated flux of 39 ± 10 Jy · km s^{-1}, which corresponds to a [O III]$_{88\ \mu m}$ luminosity of (2.1 ± 0.5) $10^8\ L_\odot$ (P. M. Solomon et al. 1992) (after correction for lensing magnification; S. Carniani et al. 2024). This places GS-z14 a factor of $\sim 2\times$ below the local relation between $L_{[O\ III]}$ and SFR for metal-poor dwarf galaxies from I. De Looze et al. (2014), albeit nearly within the scatter (Figure 3). The general consistency with the $z = 0$ relation for a galaxy a mere $\sim$300 Myr after the Big Bang suggests that GS-z14 has undergone rapid evolution, as discussed in detail in Section 4.1.

3.2. Dust Continuum

We do not detect the dust continuum from GS-z14, with a formal 90 μm continuum limit of <15.1 μJy beam^{-1} (3σ). We provide an upper limit on its dust mass assuming an optically thin modified blackbody with a dust temperature of $T_d = 60$ K and $\beta_{IR} = 2.03$ for the dust SED. The assumed temperature is consistent with extrapolations from theoretical models (e.g., L. Liang et al. 2019; L. Sommovigo et al. 2022a) and observational trends (e.g., C. Schreiber et al. 2018; A. L. Faisst et al. 2020; L. Sommovigo et al. 2021, 2022a, 2022b; J. Witstok et al. 2023a) to $z \approx 14$. We note that the precise evolution of dust temperature is still uncertain and debated (e.g., L. Sommovigo et al. 2022b). However, our assumption of a relatively high dust temperature is also supported by the inverse correlation between metallicity and dust temperature noted by L. Sommovigo et al. (2022b) and the increasing temperature of the cosmic microwave background (CMB) at high redshift.[12]

[12] For context, the CMB at $z = 14.2$ has a temperature of $T_{CMB} = 41.4$ K.

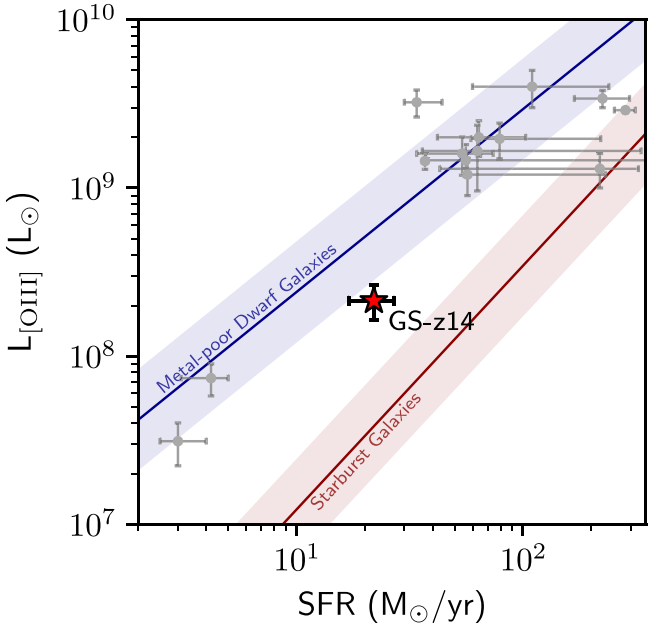

Figure 3. The luminosity of [O III]$_{88\ \mu m}$ in GS-z14 is consistent with the local relation for metal-poor dwarf galaxies found by I. De Looze et al. (2014). For context, we also show the local relation for starburst galaxies (I. De Looze et al. 2014) as well as a compilation of $z > 6.5$ galaxies (T. J. L. C. Bakx et al. 2020; S. Carniani et al. 2020; Y. Harikane et al. 2020; H. B. Akins et al. 2022; J. Witstok et al. 2022; H. S. B. Algera et al. 2024; S. Fujimoto et al. 2024). Even as early as $z = 14.1793 \pm 0.0007$ and for high redshift galaxies in general, the relation for metal-poor dwarf galaxies seems to be a good fit (at SFR $\lesssim 100\ M_\odot$ yr^{-1}).

We follow A. Ferrara et al. (2025) by adopting the J. C. Weingartner & B. T. Draine (2001) dust model with $\kappa_{88} = 34.15$ cm^{-2} g^{-1} at rest-frame 88 μm. This yields a (lensing-corrected) upper limit on the dust mass and infrared luminosity (integrated across 8–1000 μm) of $\log(M_d/M_\odot) < 6.0$ and $\log(L_{IR}/L_\odot) < 11.1$, respectively. The latter corresponds to an obscured SFR of $SFR_{IR} < 14\ M_\odot$ yr^{-1}, which, combined with the unobscured SFR of GS-z14 inferred by S. Carniani et al. (2024), implies an obscured fraction of $f_{obs} < 0.66$. Finally, using the

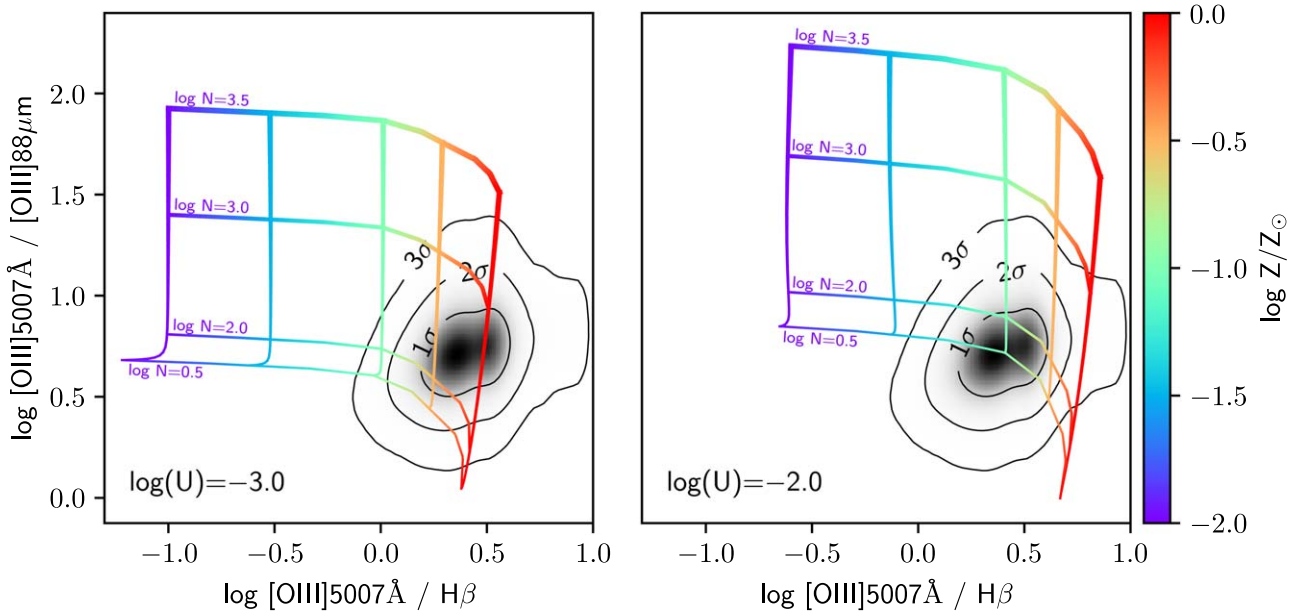

Figure 4. The ALMA and MIRI observations constrain the emission line ratios of GS-z14 to the dark shaded region in the figure highlighted by the 1σ and 2σ contours. ISM modeling, as shown by the colored grid, highlights the dependence on metallicity and density. This indicates that GS-z14 is consistent with a relatively high metallicity ($Z > 0.1\ Z_\odot$) and moderate to low density $\log(N) < 3.0\ \mathrm{cm}^{-3}$. There is a further minor dependence on the ionization parameter that shifts and deforms the grid, but does not impact the conclusions. For context, SED fitting of GS-z14 finds $\log(U) = -2.5 \pm 0.5$ (J. M. Helton et al. 2024).

stellar mass of GS-z14 inferred by J. M. Helton et al. (2024), we infer a dust-to-stellar mass ratio $\xi_d \equiv M_\mathrm{d}/M_\star < 1.9 \times 10^{-3}$.

The above estimates require the assumption of a dust temperature. Assuming a lower temperature of $T_\mathrm{d} = 45$ K, which would imply no significant evolution of the dust temperature from $z \sim 4$ (e.g., A. L. Faisst et al. 2020), results in a dust mass of $\log(M_\mathrm{d}/M_\odot) < 6.8$. Meanwhile, a significantly higher temperature of $T_\mathrm{d} = 100$ K would result in a dust mass of $\log(M_\mathrm{d}/M_\odot) < 5.3$. In Section 4.2, we discuss this in further detail, focusing on the attenuation-free model (AFM) by A. Ferrara et al. (2025), which self-consistently predicts a dust temperature for GS-z14 based on the observed V-band attenuation and the spatial extent of the dust.

4. Discussion

4.1. Constraints on the ISM of GS-z14

Luminosity ratios of emission lines are invaluable diagnostic tools to probe the conditions of the ISM in galaxies. Although the NIRSpec spectroscopy of GS-z14 does not show significant emission lines, its detection in the MIRI F770W band places a constraint on the combined [O III]$\lambda\lambda$4959,5007 Å + Hβ flux. Following J. M. Helton et al. (2024), we assume that the flux excess in F770W is 27.5 ± 5.6 nJy based on a flat underlying continuum emission.

The [O III]λ5007 Å luminosity (hereafter [O III]) can subsequently be calculated based on an assumed [O III]/Hβ ratio and can be compared to the luminosity of O III as measured by ALMA. We repeat this calculation $10^6\times$, drawing random [O III]/Hβ ratios from probability distributions from the SED fitting by J. M. Helton et al. (2024), where we combine the probability distributions from the three star formation history assumptions. This distribution has a median ratio of $2.5^{+0.9}_{-0.6}$. As noted by J. M. Helton et al. (2024), this is lower than the median [O III]/Hβ at $z \sim 8.0$, which is $6.0^{+2.4}_{-2.9}$ in JADES (J. M. Helton et al. 2024), 6.4 ± 0.9 in FRESCO (R. A. Meyer et al. 2024), and $7.2^{+2.6}_{-2.4}$ in PRIMAL (K. E. Heintz et al. 2025).

In this process, we also account for the uncertainty in the line luminosities from ALMA and JWST by drawing random values from a Gaussian error distribution.

The resulting constraints on the [O III]/[O III]$_{88\ \mu\mathrm{m}}$ versus [O III]/Hβ line ratios are shown in Figure 4. For context, we show a grid of ISM models for a large range of conditions based on Cloudy models (G. J. Ferland et al. 2017). The models consist of a H II region that smoothly transitions to a photodissociation region until a fixed optical depth ($A_V = 10$) in a plane parallel geometry. For more details on the model, we refer to J. Witstok et al. (2022). We note that the ionization parameter of GS-z14 has been loosely constrained by J. M. Helton et al. (2024) to be $\log(U_\mathrm{ion}) = -2.5 \pm 0.5$, and we therefore show two sets of CLOUDY models bracketing this range, at a fixed $\log(U_\mathrm{ion}) \in (-3.0, -2.0)$. We focus on the grid with an ionization parameter $\log(U_\mathrm{ion}) = -2$, as M. Kohandel et al. (2023) predict the most [O III]$_{88\ \mu\mathrm{m}}$-luminous galaxies at $z \gtrsim 10$ have high ionization parameters. Moreover, if the assumed [O III]/Hβ is underestimated, the observed line ratios can only be reproduced by higher values of the ionization parameter.

While the uncertainties are substantial, given the existence of only a photometric detection of the [O III]$\lambda\lambda$4959,5007 Å line, the J. Witstok et al. (2022) models suggest a relatively high metallicity of $Z \sim 0.1\ Z_\odot$, in combination with a moderate-to-low electron density ($\log N \lesssim 10^{2.5}$). This is on the low end of, albeit still consistent with, the distribution of electron densities found for $z \gtrsim 5$ galaxies, which typically show values of $\log(N) \sim 2 - 3$ (e.g., Y. Isobe et al. 2023). However, for more accurate constraints on the ISM conditions of GS-z14, direct spectroscopic detections of additional oxygen lines are crucial, for example, through MIRI spectroscopy.

Intriguingly, the detection of [O III]$_{88\ \mu\mathrm{m}}$ at $z = 14.1793 \pm 0.0007$ is consistent within 1σ with the tentative detection of C III]$\lambda\lambda$1907,9 Å reported by S. Carniani et al. (2024) at $z = 14.178 \pm 0.013$. S. Carniani et al. (2024) derive a C III] $\lambda\lambda$1907,9 Å rest-frame equivalent width (EW_0) of 8.0 ± 2.3 Å,

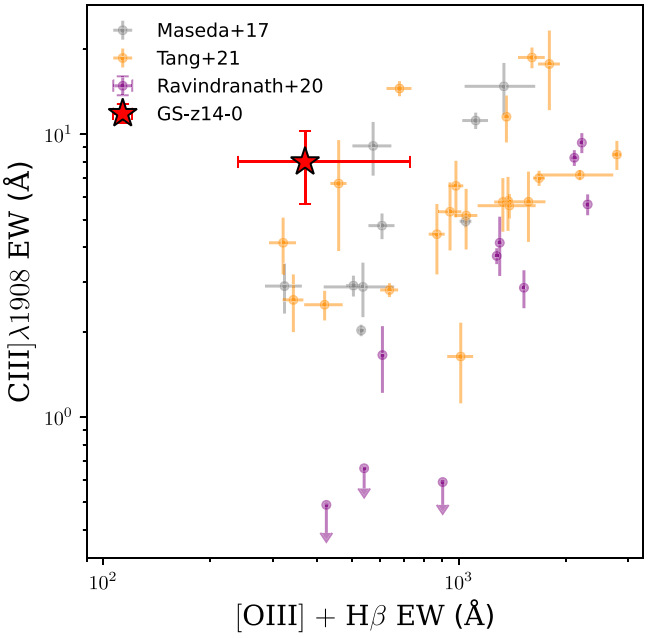

Figure 5. The rest-frame equivalent width of C III]λλ1907,9 Å as a function of EW_0([O III]+Hβ) (S. Carniani et al. 2024; J. M. Helton et al. 2024). GS-z14-0 is broadly consistent with measurements from the literature at $z = 1$–3 (gray, purple, and orange points; M. V. Maseda et al. 2017; S. Ravindranath et al. 2020; M. Tang et al. 2021).

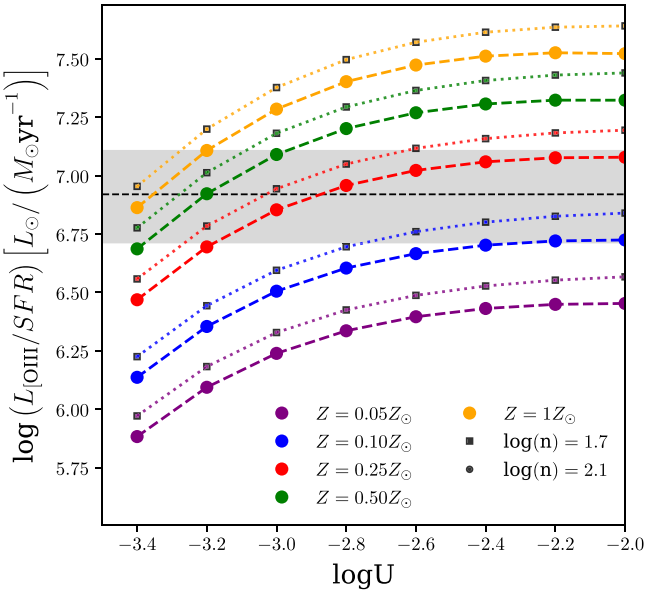

Figure 6. CLOUDY modeling of the [O III]$_{88\,\mu m}$/SFR as a function of ionization parameter for a range of metallicities and densities ∼50–100 cm^{-3}. Our model gives a lower limit on the metallicity of ∼10% $Z_\odot$, with higher gas densities and older ages preferring higher metallicity estimates.

which is relatively high compared to the EW_0([O III]+Hβ) of 370^{+360}_{-130} Å estimated by J. M. Helton et al. (2024), albeit consistent with the distribution found for galaxies at $z \sim 0$–4 (e.g., M. V. Maseda et al. 2017; S. Ravindranath et al. 2020; M. Tang et al. 2021), see Figure 5. The measured equivalent widths are in agreement with predictions from CLOUDY at a metallicity of $Z \sim 0.05$–$0.2\,Z_\odot$, and with an ionization parameter of $\log(U) \sim -2.5$, in agreement with J. M. Helton et al. (2024).

Moreover, T. Jones et al. (2020) derive a calibration for the oxygen abundance using the [O III]$_{88\,\mu m}$ line and star formation rate. Using their calibration, we derive $12 + \log O^{++}/H^{+} = 7.66^{+0.19}_{-0.21}$ (∼6%–14% solar metallicity, using the solar abundance from M. Asplund et al. 2009). In Figure 6, we use a CLOUDY grid with a 1 Myr old input stellar population to estimate the [O III]$_{88\,\mu m}$/SFR ratio as a function of ionization parameter, for models with different metallicity and gas density. For modest gas density, the measurements are consistent with 10% solar oxygen abundance; however, higher gas densities or older ages for the input stellar population will give higher metallicity estimates (up to solar metallicity).

The detection of both carbon and oxygen lines thus reinforces the notion that GS-z14 is already moderately chemically enriched. Adopting a fiducial $Z \sim 0.05$–$0.2\,Z_\odot$ in combination with the stellar mass from J. M. Helton et al. (2024), GS-z14 falls onto the high-redshift mass–metallicity relation, which has been mapped out to $z \sim 10$, and appears to show only mild evolution beyond $z \gtrsim 3$ (e.g., M. Curti et al. 2024).

4.2. Constraints on Dust Formation Processes

The build-up of dust in galaxies is a complex process involving multiple mechanisms of dust production and destruction, operating on different timescales. Supernovae (SNe) produce dust quickly, on timescales similar to the lifecycle of massive stars (∼10 Myr), while asymptotic giant branch stars contribute to dust production on significantly longer timescales (∼300 Myr; R. Schneider & R. Maiolino 2024). The contribution from grain growth in the ISM depends on the physical conditions, but is expected to be subdominant at extremely high redshifts and low gas-phase metallicities (A. Ferrara et al. 2016; P. Dayal et al. 2022; J. Witstok et al. 2023a; V. Markov et al. 2024).

At lower redshifts, it is difficult to disentangle the impact of different contributions (e.g., I. De Looze et al. 2020; F. Galliano et al. 2021), but GS-z14 has formed sufficiently early in cosmic history that dust production through SNe is likely the dominant formation process. This makes GS-z14 an ideal test-bed for dust formation models in the early Universe.

The efficiency of dust production from SNe can be inferred by measuring the dust-to-stellar-mass ratio (ξ_d). This parameter is hard to interpret as it depends on both the expected number of SNe per unit of formed stellar mass (ν), which, in turn, depends on the assumed IMF, and on the net dust yield per supernova (SN) event (y_d), $\xi_d = y_d \times \nu$. In local SN remnants, y_d values varying in the wide range from 0.01 to 1.1 $M_\odot$ have been directly measured (D. Milisavljevic et al. 2024). Such values are broadly in agreement with most indirect high-z measurements based on dust-to-stellar-mass ratios (L. Sommovigo et al. 2022a, 2022b).

Utilizing the continuum nondetection of GS-z14, we can attempt to place an upper limit on y_d. Following M. J. Michałowski (2015) and adopting a Salpeter IMF, the limit of $\xi_d < 2 \times 10^{-3}$ suggests a yield of $y_d < 0.24\,M_\odot$/SN. This is consistent with a commonly adopted yield of $y_d \sim 0.1\,M_\odot$/SN (e.g., P. Dayal et al. 2022; L. Sommovigo et al. 2022a). If we rely on such a value for $y_d \sim 0.1\,M_\odot$/SN and assume that dust follows a similar spatial distribution as the stellar component, GS-z14 should be largely obscured ($A_V \sim 9.5$; see also A. Ferrara et al. 2025) and would not have been detected with JWST. However, the JWST data only reveal

Table 1
Properties of GS-z14

Parameter	Value
R.A.	03:32:19.9049
Decl.	−27:51:20.265
Redshift	$z = 14.1793(7)$
M_{UV}	-20.81 ± 0.16
Stellar Mass ($\log(M_\odot)$)	$8.7^{+0.5}_{-0.4}$
Star Formation Rate ($M_\odot$/yr)	25^{+6}_{-5}
[O III]$_{88\ \mu m}$ Luminosity ($10^8\ L_\odot$)	2.1 ± 0.5
FWHM [O III]$_{88\ \mu m}$ (km s^{-1})	136 ± 31
Dynamical Mass ($M_\odot$ (sin i)^2)	$(1.0 \pm 0.5) \times 10^9$
90 μm continuum flux (μJy/beam)	<15.1 (3σ)
Dust Mass ($\log(M_\odot)$)	<6.0

Note. M_{UV} from S. Carniani et al. (2024); stellar mass and SFR from J. M. Helton et al. (2024). Values have been corrected for a lensing magnification of 1.17× (S. Carniani et al. 2024).

a relatively low visual extinction of $A_V = 0.31$, implying a much (1 dex) lower dust mass of $5 \times 10^4\ M_\odot$ with $\xi_d < 10^{-4}$ and $y_d < 0.015\ M_\odot$/SN (A. Ferrara et al. 2025).

Clearly, SNe (and later on growth in the ISM) do produce tangible amounts of dust, as less than 500 Myr later, at $z \approx 7$, dust appears widespread (H. Inami et al. 2022; H. S. B. Algera et al. 2023; S. Schouws et al. 2023; J. Witstok et al. 2023a)—both puzzlingly high dust-to-stellar-mass ratios ($M_d/M_\star \sim 0.01$; H. S. B. Algera et al. 2024) and fully dust-obscured sources (Y. Fudamoto et al. 2021) are observed at this epoch. In addition, features of the attenuation curve associated with the carbonaceous dust grains produced by SNe are observed at $z \sim 6.7$ (J. Witstok et al. 2023b).

The discrepancy between what is observed by JWST versus what is expected based on dust production from past SNe can be resolved by assuming that the majority of the dust has been removed from star-forming regions by radiation pressure-driven outflows. Such a scenario had been suggested in the AFM presented in A. Ferrara et al. (2025).

In their fiducial model, A. Ferrara et al. (2025) suggest the dust in GS-z14 to have a typical extent of 1.4 kpc, as a more compact size would be inconsistent with the visual extinction measured by JWST. We note that, given the resolution of our data, dust of this extent would not be resolved across multiple ALMA beams. Combined with a fiducial yield of $0.1\ M_\odot$/SN, the AFM predicts a continuum flux density for GS-z14 of $F_{88} = 14.9\ \mu$Jy. This is just below the sensitivity limit of our observations, which yield an upper limit of $F_{88} < 15.1\ \mu$Jy beam^{-1}. However, if the assumed dust yield is 0.5 dex lower ($0.1\ M_\odot$/SN), then the expected flux density would be $F_{88} \sim 8\ \mu$Jy, well below the current limit. As such, a conclusive investigation of the dust content of GS-z14, as well as further testing of the AFM model predictions, requires deeper and high-resolution ALMA continuum observations.

5. Summary

We report the robust detection of a 6.6σ [O III]$_{88\ \mu m}$ line of JADES-GS-z14-0 at 223.528 ± 0.009 GHz, providing us with a precise spectroscopic redshift measurement of $z = 14.1793 \pm 0.0007$ (see Table 1). This represents a substantial jump in redshift over the previous high-redshift [O III]$_{88\ \mu m}$-detection from MACS1149-JD1 at $z = 9.1096$ (T. Hashimoto et al. 2018). The [O III]$_{88\ \mu m}$ line was identified using data from an ALMA Cycle-10 DDT program (2023.A.00037.S, PI: Schouws) providing a spectral scan from 218.70 to 229.45 GHz (10.75 GHz baseline), covering the redshift range $z = 13.79$–14.51. The precision of the current redshift measurement represents $\gtrsim 180\times$ gain over the prior redshift measurement of $z = 14.32^{+0.08}_{-0.20}$ from NIRSpec.

The redshift we find for the source is consistent with the redshift S. Carniani et al. (2024) derive ($z = 14.178 \pm 0.013$) based on their tentative 3.6σ detection of C III]$_{1907,1909}$ doublet at 2.89 μm, providing strong evidence that the earlier line detection is real. As such, we now have multiple line detections of GS-z14-0, C III]$_{1907,1909}$ (3.6σ) with JWST and [O III]$_{88\ \mu m}$ (6.6σ) with ALMA, providing rather definitive evidence for the robustness of the redshift determination of GS-z14-0. Of note, the detection of [O III]$_{88\ \mu m}$ with ALMA was achieved with less integration time (2.8 hr) than was required for the 3.6σ tentative detection of C III]$_{1907,1909}$ with JWST (9.3 hr), providing a rather dramatic illustration of the discovery potential of ALMA.

We find no detection of the dust continuum from JADES-GS-z14-0 based on the DDT observations, with a $< 3\sigma$ upper limit of $<15.1\ \mu$Jy beam^{-1}. This suggests a low dust-to-stellar-mass ratio of $M_d/M_\star < 1.9 \times 10^{-3}$, consistent with supernova dust production yields $y_d < 0.24\ M_\odot$/SN.

Combining a previous JWST/MIRI photometric measurement of the [O III]$\lambda\lambda$4959,5007 Å and Hβ lines with CLOUDY models, we find GS-z14 to be surprisingly metal-enriched ($Z \sim 0.05$–$0.2\ Z_\odot$) a mere 300 Myr after the Big Bang, with moderate to low density $\log(N) < 3.0$ cm^{-3}.

Thanks to the precise spectroscopic redshift measurement and [O III]$_{88\ \mu m}$ line detection we now have for GS-14-0 using just 2.8 hr, it is clear that additional follow-up of GS-z14-0 with ALMA would be highly fruitful and should include (1) higher spatial resolution observations of [O III]$_{88\ \mu m}$ to improve constraints on dynamical masses and state of GS-z14-0 and deeper constraints on the dust continuum, (2) observations of the [C II]$_{158\ \mu m}$ line in Band 4, lying just 0.2 GHz above the low-frequency boundary, to better probe the ionization parameter U and build-up of metals, and (3) JWST/MIRI observations of [O III]$\lambda\lambda$4959,5007 Å and Hβ to place tighter constraints on the electron density and metallicity of GS-z14-0.

Acknowledgments

This paper makes use of the following ALMA data: ADS/JAO.ALMA 2023.A.00037.S. ALMA is a partnership of ESO (representing its member states), NSF (USA) and NINS (Japan), together with NRC (Canada), MOST and ASIAA (Taiwan), and KASI (Republic of Korea), in cooperation with the Republic of Chile. The Joint ALMA Observatory is operated by ESO, AUI/NRAO, and NAOJ. We are greatly appreciative to our ALMA program coordinator Violette Impellizzeri for support with our ALMA program and Allegro, the European ALMA Regional Center node in the Netherlands. We are grateful to J. Witstok for providing the CLOUDY models from J. Witstok et al. (2022) for the analysis conducted in this paper. We thank M. Kohandel and A. Pallottini for simulated data analysis. This work was supported by NAOJ ALMA Scientific Research grant Code 2021-19A (HA). A.F. acknowledges support from the ERC Advanced grant INTERSTELLAR H2020/740120 and support from the grant NSF PHY-2309135 to the Kavli Institute for Theoretical Physics (KITP).

ORCID iDs

Sander Schouws https://orcid.org/0000-0001-9746-0924
Rychard J. Bouwens https://orcid.org/0000-0002-4989-2471
Katherine Ormerod https://orcid.org/0000-0003-2000-3420
Hiddo Algera https://orcid.org/0000-0002-4205-9567
Laura Sommovigo https://orcid.org/0000-0002-2906-2200
Jacqueline Hodge https://orcid.org/0000-0001-6586-8845
Andrea Ferrara https://orcid.org/0000-0002-9400-7312
Pascal A. Oesch https://orcid.org/0000-0001-5851-6649
Lucie E. Rowland https://orcid.org/0009-0009-2671-4160
Ivana van Leeuwen https://orcid.org/0009-0005-6803-6805
Mauro Stefanon https://orcid.org/0000-0001-7768-5309
Thomas Herard-Demanche https://orcid.org/0000-0003-2164-7949
Yoshinobu Fudamoto https://orcid.org/0000-0001-7440-8832
Huub Röttgering https://orcid.org/0000-0001-8887-2257
Paul van der Werf https://orcid.org/0000-0002-4389-832X

References

Akins, H. B., Fujimoto, S., Finlator, K., et al. 2022, ApJ, 934, 64
Algera, H. S. B., Inami, H., Oesch, P. A., et al. 2023, MNRAS, 518, 6142
Algera, H. S. B., Inami, H., Sommovigo, L., et al. 2024, MNRAS, 527, 6867
ALMA Technical Handbook 2024, ALMA Technical Handbook, ALMA Doc. 11.3, v1.4, Zenodo, doi:10.5281/zenodo.4511521
Arata, S., Yajima, H., Nagamine, K., Abe, M., & Khochfar, S. 2020, MNRAS, 498, 5541
Asplund, M., Grevesse, N., Sauval, A. J., & Scott, P. 2009, ARA&A, 47, 481
Bakx, T. J. L. C., Tamura, Y., Hashimoto, T., et al. 2020, MNRAS, 493, 4294
Bakx, T. J. L. C., Zavala, J. A., Mitsuhashi, I., et al. 2023, MNRAS, 519, 5076
Béthermin, M., Fudamoto, Y., Ginolfi, M., et al. 2020, A&A, 643, A2
Bouwens, R., Illingworth, G., Oesch, P., et al. 2023, MNRAS, 523, 1009
Bouwens, R. J., Smit, R., Schouws, S., et al. 2022, ApJ, 931, 160
Bunker, A. J., Saxena, A., Cameron, A. J., et al. 2023, A&A, 677, A88
Carniani, S., Ferrara, A., Maiolino, R., et al. 2020, MNRAS, 499, 5136
Carniani, S., Hainline, K., D'Eugenio, F., et al. 2024, Natur, 633, 318
Castellano, M., Fontana, A., Treu, T., et al. 2022, ApJL, 938, L15
Castellano, M., Napolitano, L., Fontana, A., et al. 2024, ApJ, 972, 143
Chabrier, G. 2003, PASP, 115, 763
Cormier, D., Madden, S. C., Lebouteiller, V., et al. 2015, A&A, 578, A53
Curti, M., Maiolino, R., Curtis-Lake, E., et al. 2024, A&A, 684, A75
Curtis-Lake, E., Carniani, S., Cameron, A., et al. 2023, NatAs, 7, 622
Dayal, P., Ferrara, A., Sommovigo, L., et al. 2022, MNRAS, 512, 989
De Looze, I., Cormier, D., Lebouteiller, V., et al. 2014, A&A, 568, A62
De Looze, I., Lamperti, I., Saintonge, A., et al. 2020, MNRAS, 496, 3668
Donnan, C. T., McLeod, D. J., Dunlop, J. S., et al. 2022, MNRAS, 518, 6011
Eisenstein, D. J., Willott, C., Alberts, S., et al. 2023a, arXiv:2306.02465
Eisenstein, D. J., Johnson, B. D., Robertson, B., et al. 2023b, arXiv:2310.12340
Faisst, A. L., Fudamoto, Y., Oesch, P. A., et al. 2020, MNRAS, 498, 4192
Faisst, A. L., Schaerer, D., Lemaux, B. C., et al. 2020, ApJS, 247, 61
Ferland, G. J., Chatzikos, M., Guzmán, F., et al. 2017, RMxAA, 53, 385
Ferrara, A. 2024, A&A, 689, A310
Ferrara, A., Carniani, S., di Mascia, F., et al. 2025, A&A, 694, A215
Ferrara, A., Viti, S., & Ceccarelli, C. 2016, MNRAS, 463, L112
Finkelstein, S. L., Leung, G. C. K., Bagley, M. B., et al. 2024, ApJL, 969, L2
Fudamoto, Y., Oesch, P. A., Schouws, S., et al. 2021, Natur, 597, 489
Fujimoto, S., Finkelstein, S. L., Burgarella, D., et al. 2023, ApJ, 955, 130
Fujimoto, S., Ouchi, M., Nakajima, K., et al. 2024, ApJ, 964, 146
Furlanetto, S. R., & Mirocha, J. 2023, MNRAS, 523, 5274
Galliano, F., Nersesian, A., Bianchi, S., et al. 2021, A&A, 649, A18
Genzel, R., Tacconi, L. J., Gracia-Carpio, J., et al. 2010, MNRAS, 407, 2091
Hainline, K. N., Johnson, B. D., Robertson, B., et al. 2024, ApJ, 964, 71
Harikane, Y., Ouchi, M., Inoue, A. K., et al. 2020, ApJ, 896, 93
Harikane, Y., Ouchi, M., Oguri, M., et al. 2023, ApJS, 265, 5
Harikane, Y., Inoue, A. K., Ellis, R. S., et al. 2025, ApJ, 980, 138
Hashimoto, T., Laporte, N., Mawatari, K., et al. 2018, Natur, 557, 392
Heintz, K. E., Brammer, G. B., Watson, D., et al. 2025, A&A, 693, A60
Helton, J. M., Rieke, G. H., Alberts, S., et al. 2024, NatAs, in press
Hunter, T. R., Indebetouw, R., Brogan, C. L., et al. 2023, PASP, 135, 074501
Inami, H., Algera, H. S. B., Schouws, S., et al. 2022, MNRAS, 515, 3126
Isobe, Y., Ouchi, M., Nakajima, K., et al. 2023, ApJ, 956, 139
Jones, T., Sanders, R., Roberts-Borsani, G., et al. 2020, ApJ, 903, 150
Kaasinen, M., van Marrewijk, J., Popping, G., et al. 2023, A&A, 671, A29
Katz, H., Kimm, T., Sijacki, D., & Haehnelt, M. G. 2017, MNRAS, 468, 4831
Katz, H., Galligan, T. P., Kimm, T., et al. 2019, MNRAS, 487, 5902
Katz, H., Rosdahl, J., Kimm, T., et al. 2022, MNRAS, 510, 5603
Kepley, A. A., Tsutsumi, T., Brogan, C. L., et al. 2020, PASP, 132, 024505
Kohandel, M., Ferrara, A., Pallottini, A., et al. 2023, MNRAS, 520, L16
Le Fèvre, O., Béthermin, M., Faisst, A., et al. 2020, A&A, 643, A1
Liang, L., Feldmann, R., Kereš, D., et al. 2019, MNRAS, 489, 1397
Markov, V., Gallerani, S., Ferrara, A., et al. 2024, NatAs, in press
Maseda, M. V., Brinchmann, J., Franx, M., et al. 2017, A&A, 608, A4
Meyer, R. A., Oesch, P. A., Giovinazzo, E., et al. 2024, MNRAS, 535, 1067
Michałowski, M. J. 2015, A&A, 577, A80
Milisavljevic, D., Temim, T., Looze, I. D., et al. 2024, ApJL, 965, L27
Moriwaki, K., Yoshida, N., Shimizu, I., et al. 2018, MNRAS, 481, L84
Naidu, R. P., Oesch, P. A., van Dokkum, P., et al. 2022, ApJL, 940, L14
Nakazato, Y., Yoshida, N., & Ceverino, D. 2023, ApJ, 953, 140
Oesch, P. A., Brammer, G., Dokkum, P. G. v., et al. 2016, ApJ, 819, 129
Oesch, P. A., Brammer, G., Naidu, R. P., et al. 2023, MNRAS, 525, 2864
Oke, J. B., & Gunn, J. E. 1983, ApJ, 266, 713
Pallottini, A., Ferrara, A., Gallerani, S., et al. 2022, MNRAS, 513, 5621
Popping, G. 2023, A&A, 669, L8
Ravindranath, S., Monroe, T., Jaskot, A., Ferguson, H. C., & Tumlinson, J. 2020, ApJ, 896, 170
Robertson, B. E., Tacchella, S., Johnson, B. D., et al. 2023, NatAs, 7, 611
Santini, P., Fontana, A., Castellano, M., et al. 2023, ApJL, 942, L27
Schneider, R., & Maiolino, R. 2024, A&ARv, 32, 2
Schouws, S., Stefanon, M., Bouwens, R., et al. 2022, ApJ, 928, 31
Schouws, S., Bouwens, R., Smit, R., et al. 2023, ApJ, 954, 103
Schreiber, C., Elbaz, D., Pannella, M., et al. 2018, A&A, 609, A30
Solomon, P. M., Downes, D., & Radford, S. J. E. 1992, ApJL, 387, L55
Sommovigo, L., Ferrara, A., Carniani, S., et al. 2021, MNRAS, 503, 4878
Sommovigo, L., Ferrara, A., Pallottini, A., et al. 2022a, MNRAS, 513, 3122
Sommovigo, L., Ferrara, A., Carniani, S., et al. 2022b, MNRAS, 517, 5930
Tang, M., Stark, D. P., Chevallard, J., et al. 2021, MNRAS, 501, 3238
Thompson, A. R., Moran, J. M., & Swenson, G. W. J. 2017, Interferometry and Synthesis in Radio Astronomy (3rd ed.; Cham: Springer)
Treu, T., Calabró, A., Castellano, M., et al. 2023, ApJL, 942, L28
Vallini, L., Ferrara, A., Pallottini, A., Carniani, S., & Gallerani, S. 2021, MNRAS, 505, 5543
Vallini, L., Witstok, J., Sommovigo, L., et al. 2024, MNRAS, 527, 10
Weingartner, J. C., & Draine, B. T. 2001, ApJ, 548, 296
Williams, C. C., Alberts, S., Ji, Z., et al. 2024, ApJ, 968, 34
Witstok, J., Jones, G. C., Maiolino, R., Smit, R., & Schneider, R. 2023a, MNRAS, 523, 3119
Witstok, J., Smit, R., Maiolino, R., et al. 2022, MNRAS, 515, 1751
Witstok, J., Shivaei, I., Smit, R., et al. 2023b, Natur, 621, 267
Yang, S., & Lidz, A. 2020, MNRAS, 499, 3417
Yoon, I., Carilli, C. L., Fujimoto, S., et al. 2023, ApJ, 950, 61
Zavala, J. A., Castellano, M., Akins, H. B., et al. 2024, NatAs, 9, 155